

Diversity of electronic transitions and photoluminescence properties in nanocrystalline Mn/Fe-doped tin dioxide semiconductor films: An effect from oxygen pressure

W. L. Yu, W. W. Li, J. D. Wu, J. Sun, Z. G. Hu et al.

Citation: *J. Appl. Phys.* 110, 123502 (2011); doi: 10.1063/1.3669374

View online: <http://dx.doi.org/10.1063/1.3669374>

View Table of Contents: <http://jap.aip.org/resource/1/JAPIAU/v110/i12>

Published by the [American Institute of Physics](#).

Related Articles

Excitation power and temperature dependence of excitons in CuInSe₂
[J. Appl. Phys.](#) 111, 093507 (2012)

Effect of Li-doping on the magnetic properties of ZnO with Zn vacancies
[J. Appl. Phys.](#) 111, 093902 (2012)

Optically controlled spin-dependent Andreev reflection and spin accumulation in a quantum dot
[J. Appl. Phys.](#) 111, 083706 (2012)

Thermal emission in type-II GaSb/GaAs quantum dots and prospects for intermediate band solar energy conversion
[J. Appl. Phys.](#) 111, 074514 (2012)

Ab initio calculation of the CdSe/CdTe heterojunction band offset using the local-density approximation-1/2 technique with spin-orbit corrections
[J. Appl. Phys.](#) 111, 073708 (2012)

Additional information on J. Appl. Phys.

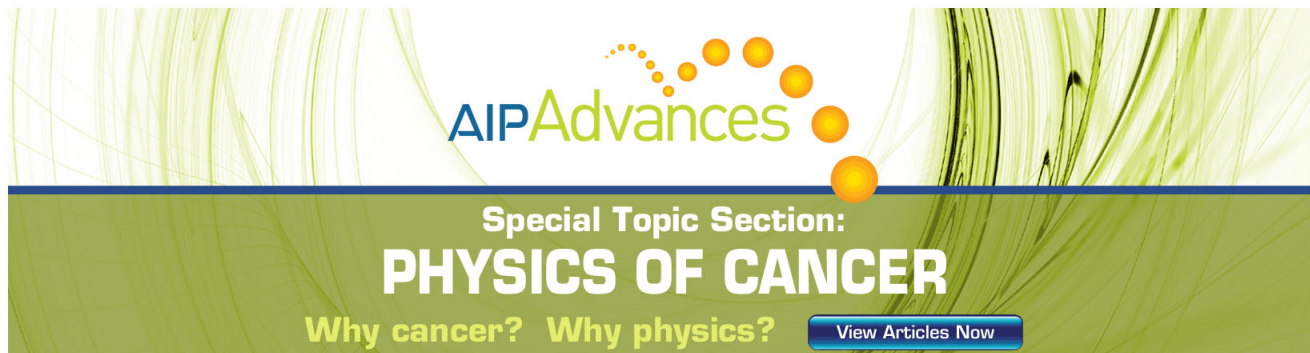
Journal Homepage: <http://jap.aip.org/>

Journal Information: http://jap.aip.org/about/about_the_journal

Top downloads: http://jap.aip.org/features/most_downloaded

Information for Authors: <http://jap.aip.org/authors>

ADVERTISEMENT



The advertisement banner features a green and white abstract background with flowing lines. At the top center, the text "AIPAdvances" is displayed in a green, sans-serif font, with a decorative arc of orange and yellow circles above it. Below this, the text "Special Topic Section:" is written in white, followed by "PHYSICS OF CANCER" in large, bold, white capital letters. At the bottom left, the phrase "Why cancer? Why physics?" is written in a light green font. On the bottom right, there is a blue button with white text that reads "View Articles Now".

Diversity of electronic transitions and photoluminescence properties in nanocrystalline Mn/Fe-doped tin dioxide semiconductor films: An effect from oxygen pressure

W. L. Yu (余温雷),¹ W. W. Li (李文武),¹ J. D. Wu (吴嘉达),² J. Sun (孙剑),² Z. G. Hu (胡志高),^{1,a)} and J. H. Chu (褚君浩)¹

¹Key Laboratory of Polar Materials and Devices, Ministry of Education, Department of Electronic Engineering, East China Normal University, Shanghai 200241, People's Republic of China

²Key Laboratory for Advanced Photonic Materials and Devices, Ministry of Education, Department of Optical Science and Engineering, Fudan University, Shanghai 200433, People's Republic of China

(Received 3 June 2011; accepted 12 November 2011; published online 19 December 2011; publisher error corrected 23 December 2011)

Transition metal (TM: Mn or Fe) doped tin dioxide (SnO₂) films with the compositions of 5% (Sn_{0.95}TM_{0.05}O₂) have been deposited on sapphire substrates by pulsed laser deposition under oxygen pressure (P_o) varied from 10⁻⁴ to 1 Pa. The x-ray diffraction, scanning electron microscopy, and infrared spectra analysis show that different TM dopants can affect the variations of crystallization and lattice distortion. Moreover, x-ray photoelectron spectroscopies indicate that the effective P_o during the growth does not change the valence state of Sn⁴⁺ in the Sn_{0.95}TM_{0.05}O₂ films. The spectral behaviors of the films have been investigated in the photon energy range of 0.47–6.5 eV (2650–190 nm). From transmittance spectra, the shoulder structures become more prominent for the Sn_{0.95}Fe_{0.05}O₂ film than those for the Sn_{0.95}Mn_{0.05}O₂ film due to the Fe repelling effect of a stronger p-d hybridization. The refractive index values for the Sn_{0.95}Mn_{0.05}O₂ film are found to be larger than those for the Sn_{0.95}Fe_{0.05}O₂ film at the photon energy of 0.47 eV. The main peaks at about 1.9 and 2.2 eV in photoluminescence (PL) emission spectra for both Sn_{0.95}Mn_{0.05}O₂ and Sn_{0.95}Fe_{0.05}O₂ films can be observed, and it could be explained by the fact that the electrons in the conduction band of SnO₂ relax to defect states and then radiatively recombine with the holes. From direct comparison of PL and transmittance results for the films, the electronic transition energies, the emission peaks' intensities and positions are shown to present the P_o dependent behavior. The distinct trends indicate that the incorporation of Mn and Fe elements can provide a significant difference in the crystalline and electronic band structure. It can be concluded that the oxygen pressure and dopant contributions are responsible for the adjustment of electronic band structures and result in different optical response behaviors for the Sn_{0.95}TM_{0.05}O₂ films. © 2011 American Institute of Physics. [doi:10.1063/1.3669374]

I. INTRODUCTION

Tin dioxide (SnO₂) is one of the most used key functional materials, which has two structural characteristics: cations with mixed valence states and anions with deficiencies. By varying either or both of these characteristics, the electrical, optical, and magnetic properties can be modified, giving the possibility of fabricating optoelectronic devices, transparent conducting electrodes, gas sensors for detecting leakages, and catalyst supports.^{1,2} In particular, SnO₂ doped with transition metal (TM) ion, such as Fe, Mn, Ni, Co, etc., has been extensively studied because of its excellent optical transparency, high refractive index, tunable carrier concentration, and diluted magnetic semiconductor.^{3,4} Theoretical calculations predict that ferromagnetism is the ground state and the Curie temperature is expected to have a higher value for Fe doped SnO₂. However, paramagnetism is more stable than ferromagnetism in Mn doped SnO₂. Moreover, TM-oxygen vacancy-TM groups can be formed in Fe doped SnO₂, but the phenomenon does not appear in the cases of Mn doping.⁵ Considering the different effects from the

doping TM elements, it is interesting to investigate the electronic band structures of Mn and Fe doped SnO₂ by a comparison with their optical properties.

Spectral and photoluminescence (PL) measurements are highly helpful to investigate optoelectronic properties of the nanostructured films, which are affected by the structure defects and impurity levels of the material.⁶ For the oxide materials, many physical properties are driven by defects, which are mostly due to the varied oxygen content. It has been calculated that removal of the bridging O atoms leads to the formation of a dispersed band within the forbidden band gap, which is the cause of oxygen vacancies. The removal of the in-plane oxygen atoms, however, can induce the formation of a single defect level above the valence band.^{7,8} Furthermore, oxygen vacancies are extremely important for determining the electrical conductivity of SnO₂,⁷ and they are also responsible for an efficient luminescence activity in SnO₂ nanocrystalline. Intense and orange light emission from SnO₂ nanostructures has recently been found, suggesting that SnO₂ may be a promising candidate for luminescent materials.^{2,9} Although there are the remarkable attentions on SnO₂-based semiconductors, the experimental results reported by different research groups have been

^{a)}Author to whom correspondence should be addressed. Electronic mail: zgghu@ee.ecnu.edu.cn.

frequently controversial on the origin of PL emission properties.

It is known that a given material preparation method has strong effect on the microstructure and physical properties. As compared with other deposition methods, pulsed laser deposition (PLD) technique has the ability to exceed the solubility of magnetic impurity and to permit high quality film grown at low substrate temperature.¹⁰ Additionally, PLD is done in high vacuum and allows precise control of background reactive gas pressure. Oxygen is one of the common background sources and affects the sample growth in the PLD process because it is a major constitute of oxides. Moreover, the first principle calculation also shows that the oxygen vacancy and tin interstitial can be easily induced due to surprisingly low formation energies and strong mutual interactions.¹¹ Thus understanding the role of surrounding oxygen is essential to the microstructure and properties of the oxides. Up to date, it has been reported that the crystallinity and PL property for ZnO strongly depend on the oxygen pressure (P_o).¹² Some groups also discussed the effect of oxygen concentration on structure and ferromagnetism for SnO₂ nanoparticles,^{9,13} and the PL emission was found to be sensitive to the oxygen concentration.⁹ Nevertheless, systematical experimental works to reveal the P_o dependence of optical response behaviors in TM (Mn or Fe) doped SnO₂, especially a contrast to the two kinds of films, are very limited. Therefore, it is desirable to carry out a delicate study regarding the mutual correlation between the magnetic elements and oxygen levels in the TM doped SnO₂ materials.

In this paper, comprehensive characterizations are performed to explore the morphology, crystallinity, and the chemical states of the TM (Mn or Fe) doped SnO₂ films with the compositions of 5% (Sn_{0.95}TM_{0.05}O₂) prepared under varied P_o values. We demonstrate the crucial role of surrounding oxygen on electronic band structures and optical properties by means of infrared (IR) reflectance, ultraviolet-near-infrared (UV-NIR) transmittance, and PL spectra. The comparative study on the Sn_{0.95}Mn_{0.05}O₂ and Sn_{0.95}Fe_{0.05}O₂ films will be presented and oxygen vacancy contribution associated with the 3d dopants will be discussed in detail.

II. EXPERIMENTAL DETAILS

A. Preparation of the Sn_{0.95}TM_{0.05}O₂ films

The Sn_{0.95}TM_{0.05}O₂ (TM: Mn or Fe) targets in the diameter of 3 cm were prepared using a conventional solid-state reaction sintering. During the preparation, MnO or Fe₂O₃ powder was mixed with SnO₂ powder (99.99%) in which Mn or Fe mole fraction was 5%, then corresponding target of Sn_{0.95}Mn_{0.05}O₂ or Sn_{0.95}Fe_{0.05}O₂ was obtained. In order to obtain better crystalline quality, double-side polished *c*-sapphire wafers were used as the substrates. The substrates were rigorously cleaned in pure ethanol with an ultrasonic bath and were rinsed several times by de-ionized water before the deposition. Finally, the wafers were dried in a pure nitrogen stream before the deposition of the films. The PLD growth chamber was first pumped down to a base pressure of 10⁻⁴ Pa for the Sn_{0.95}TM_{0.05}O₂ films fabrication. The Sn_{0.95}TM_{0.05}O₂ films were grown at a substrate temperature of

about 450 °C and deposited in vacuum ($\sim 10^{-4}$ Pa) or in O₂ ambient at total pressures of 10⁻², 10⁻¹, and 1 Pa without any buffer gas, respectively. A Q-switched pulse yttrium aluminum garnet (Nd:YAG) laser with the wavelength of 532 nm and duration of 5 ns, which works at the repetition rate of 10 Hz and an energy of 40 mJ/pulse, was used for the target ablation. The films were grown immediately after the target was preablated. The distance between the target and substrate was kept at 3 cm and the deposition time was set to about 30 min. Then during the post-annealing process, the substrate temperature of the films was maintained at 900 °C in air atmosphere for 30 min.

B. Sample characterizations

The crystalline structures of the Sn_{0.95}TM_{0.05}O₂ (TM: Mn or Fe) films on *c*-sapphire substrates were analyzed by x-ray diffraction (XRD) using Cu $K\alpha$ radiation (D/MAX-2550 V, Rigaku Co.). In the XRD measurement, a vertical goniometer (Model RINT2000) and continuous scanning mode (θ - 2θ) were selected with a scanning rate of 10°/min and interval of 0.02°. The surface and cross-sectional microstructures of the films were studied by scanning electron microscopy (SEM). The x-ray photoelectron spectroscopic (XPS) experiments were carried out on a RBD upgraded PHI-5000C ESCA system (Perkin Elmer) with Mg $K\alpha$ radiation ($h\nu = 1253.6$ eV). Because the sapphire substrate is not transparent in the IR region, the near-normal incident ($\sim 10^\circ$) reflectance spectra were collected over the frequency range from 200 to 1200 cm⁻¹ using a Fourier transform infrared spectrometer (Bruker Vertex 80V). Gold and aluminum mirrors, whose absolute reflectances were measured, were taken as the references for the spectra in the high and low frequency regions, respectively. The spectral transmittance experiments were carried out with a double beam spectrophotometer (PerkinElmer Lambda 950) from 190 to 2650 nm (0.47-6.5 eV) with a spectral resolution of 2 nm. The PL spectra were recorded by a Jobin-Yvon LabRAM HR 800 ultraviolet spectrometer with a He-Cd laser as the excited light, which is operated at the wavelength of 325 nm (3.82 eV). Note that the experiments were carried out at room temperature and no smoothing was performed.

III. RESULTS AND DISCUSSIONS

A. Structural and morphology analysis

The XRD characterization of the Sn_{0.95}TM_{0.05}O₂ films with different P_o reveals the tetragonal rutile structure of SnO₂, as shown in Fig. 1. The peaks suggest that the films are polycrystalline. With increasing the P_o values, the intensity of (110) diffraction peak for the Sn_{0.95}Mn_{0.05}O₂ film increases but that for the Sn_{0.95}Fe_{0.05}O₂ film decreases until the pressure reaches 10⁻¹ Pa. Moreover, there are the (110) preferred orientation under the maximum P_o value of 1 Pa, while the intensity of (101) diffraction peak becomes compared to that of (110) diffraction peak under the low P_o in the present work. It is necessary to point out that the peak at Bragg angle of about 18.4° can be observed for the Sn_{0.95}Mn_{0.05}O₂ films with the P_o of 10⁻² and 10⁻¹ Pa, identified as the (001) diffraction

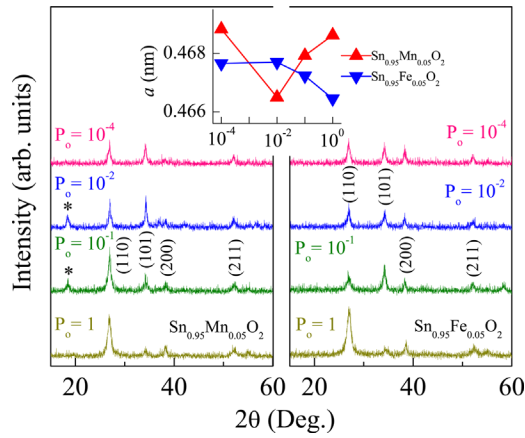


FIG. 1. (Color online) The XRD patterns of the $\text{Sn}_{0.95}\text{TM}_{0.05}\text{O}_2$ (TM: Mn or Fe) films with different oxygen pressure. The diffraction peak at about 18.4° in the $\text{Sn}_{0.95}\text{Mn}_{0.05}\text{O}_2$ films with the oxygen pressure of 10^{-2} and 10^{-1} Pa, ascribed to the tetragonal phase of SnO, is remarked by label (*). The inset shows the variation of the a -axis lattice constants evaluated from the diffraction peak (110) as the oxygen pressure.

peak for the tetragonal phase of SnO (remarked with *). However, the additional peak cannot be found for the $\text{Sn}_{0.95}\text{Fe}_{0.05}\text{O}_2$ films. The a -axis lattice constant in the inset of Fig. 1, determined using the (110) diffraction peak, shows a different variation trend with the P_o for the Mn and Fe doping films, respectively. The deviation indicates the different crystalline formation with the varied P_o because of the dopant contributions. Moreover, the average values of the a -axis lattice constant are estimated to be about 4.68 \AA and 4.67 \AA for the $\text{Sn}_{0.95}\text{Mn}_{0.05}\text{O}_2$ and $\text{Sn}_{0.95}\text{Fe}_{0.05}\text{O}_2$ films, respectively. Both of them are much smaller than those reported SnO₂ with doped by 5% Mn (4.72 \AA) or Fe (4.73 \AA and 4.79 \AA) using other preparation methods,^{14,15} which can be ascribed to different deposition technique, crystallinity, and lattice mismatch with the substrate. According to the Scherrer equation, the average crystallite sizes of the $\text{Sn}_{0.95}\text{Mn}_{0.05}\text{O}_2$ and $\text{Sn}_{0.95}\text{Fe}_{0.05}\text{O}_2$ films are about 14 and 12 nm, respectively. During the PLD process with the varied P_o , the oxygen content in all samples can be considered to be changed and the remarkable discrepancy of above structure parameters for the $\text{Sn}_{0.95}\text{TM}_{0.05}\text{O}_2$ films could be related to the P_o effect and its interaction with the dopants.

Fig. 2 presents the surface and cross-sectional SEM images from the $\text{Sn}_{0.95}\text{TM}_{0.05}\text{O}_2$ films deposited under the P_o of 10^{-1} Pa. Note that both the samples present the uniform granular structures on the sapphire substrates. Nevertheless, the $\text{Sn}_{0.95}\text{Fe}_{0.05}\text{O}_2$ film seems to contain a rough surface and dense topography. Also, the films with the Fe doping are of the distinct interface between the film and substrate, as compared to those from the $\text{Sn}_{0.95}\text{Mn}_{0.05}\text{O}_2$ films. The results suggest that different doping elements could directly affect the crystalline structure and surface morphology of the films. From the cross-sectional SEM image, the thickness of the selected films is evaluated to about several tens of nanometers, which is similar to the values obtained in fitting process. Therefore, it can be concluded that the presence of Fe or Mn could provide a strong relation to the oxygen level and a different perturbation in the structures for the $\text{Sn}_{0.95}\text{TM}_{0.05}\text{O}_2$ films, which is further supported by the following analysis.

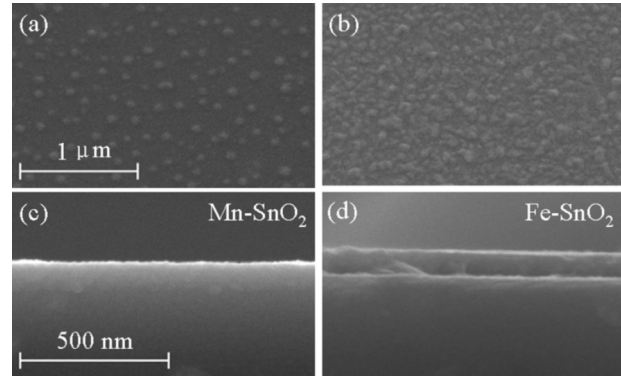


FIG. 2. (a) and (b) Surface and (c) and (d) cross-sectional SEM images of the Mn and Fe doped SnO₂ films grown under oxygen pressure of 10^{-1} Pa, respectively. Note that the given scales in the pictures (b) and (d) are $1 \mu\text{m}$ and 500 nm , respectively.

B. XPS of the $\text{Sn}_{0.95}\text{TM}_{0.05}\text{O}_2$ films

Elemental composition and chemical states of the $\text{Sn}_{0.95}\text{TM}_{0.05}\text{O}_2$ films were studied by XPS measurements. The survey spectra for all films indicate that only C 1s, Sn 3d, O 1s, and TM 2p related core levels can be detectable. The C 1s peak at 284.6 eV is used as an internal standard, and the other spectra are calibrated with the C 1s peak to correct the binding energy position. For example, high resolution spectra of Sn 3d and TM 2p for the films grown under the P_o of 10^{-1} Pa are shown in Fig. 3, and the given atomic percentages of Mn and Fe are 5.66% and 4.95% , respectively. The peaks at binding energies of $486.6/486.4 \text{ eV}$ (Sn $3d_{5/2}$) and $495/494.8 \text{ eV}$ (Sn $3d_{3/2}$) for the Mn/Fe doped film with a spin-orbit splitting of 8.4 eV can be observed in Fig. 3(a), which is in good agreement with the findings for the Sn^{4+} bound to oxygen in the matrix.⁹ In addition, all values of Sn 3d for the $\text{Sn}_{0.95}\text{TM}_{0.05}\text{O}_2$ films (see Table I) are close

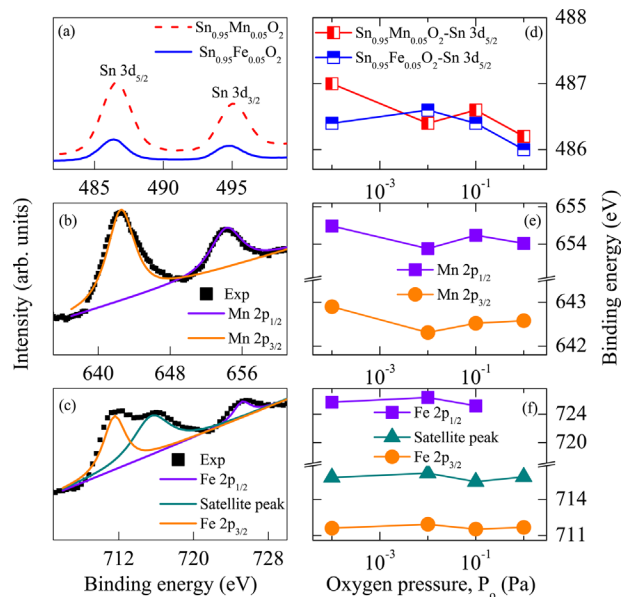


FIG. 3. (Color online) XPS spectra of the (a) Sn 3d, (b) Mn 2p, and (c) Fe 2p regions for the $\text{Sn}_{0.95}\text{TM}_{0.05}\text{O}_2$ films prepared with oxygen pressure of 10^{-1} Pa. (d), (e), and (f) Oxygen pressure dependence of the corresponding binding energy positions.

TABLE I. Comparison of binding energies from Sn 3d, O 1s, and TM 2p for various oxygen pressures in the $\text{Sn}_{0.95}\text{TM}_{0.05}\text{O}_2$ (TM: Mn or Fe) films and the peak positions of photoluminescence spectra are determined from the Gaussian fitting.

Samples	P_o (Pa)	Sn3d		O 1s		TM 2p			PL		
		$3d_{5/2}$ (eV)	$3d_{3/2}$ (eV)	O1 (eV)	O2 (eV)	$2p_{3/2}$ (eV)	$2p_{1/2}$ (eV)	Satellite peak (eV)	$P_{\text{TM}-1}$ (eV)	$P_{\text{TM}-2}$ (eV)	$P_{\text{TM}-3}$ (eV)
A _{Mn}	10^{-4}	487	495.4	530.8	532.1	642.9	654.5	—	1.956	2.277	1.551
B _{Mn}	10^{-2}	486.4	495	530.2	531.5	642.3	653.9	—	1.896	2.271	1.548
C _{Mn}	10^{-1}	486.6	495	530.2	531.5	642.5	654.2	—	1.864	2.239	1.539
D _{Mn}	1	486.2	494.8	530.2	531.6	642.6	654	—	1.903	2.267	1.565
A _{Fe}	10^{-4}	486.4	494.8	530.4	526.5	711.6	725.7	715.8	1.786	2.078	2.997
B _{Fe}	10^{-2}	486.6	495	529.9	528	711.9	726.3	716.2	1.942	2.233	2.877
C _{Fe}	10^{-1}	486.4	494.8	530.5	527	711.5	725.2	715.5	1.942	2.269	2.855
D _{Fe}	1	486	494.6	530	528.2	711.7	—	715.9	1.875	2.232	2.953

to the reported data,^{16–18} indicating that the effective oxygen pressure during the growth does not change the valence state of Sn^{4+} in the TM doping SnO_2 films. This phenomena have also been found in the literatures.^{9,19} It is known that oxygen vacancy creates a charge imbalance, so there is a possibility to generate Sn^{2+} . However, the amount of Sn^{2+} ions is very small compared with that of Sn^{4+} and below the detection limitation of the instrument. Because the Sn $3d_{5/2}$ peak exhibits only one symmetric lineshape without any shoulder, and the observed peaks in the XRD pattern have been mostly indexed with the rutile-type tetragonal structure of SnO_2 . From the above views, even though the samples were grown under different oxygen pressure, the chemical state of Sn^{4+} in the $\text{Sn}_{0.95}\text{TM}_{0.05}\text{O}_2$ films was still predominant.

The deconvolution of the O 1s XPS spectra for the $\text{Sn}_{0.95}\text{TM}_{0.05}\text{O}_2$ films are fitted by two components and the complicated results are provided in Table I and Fig. 4. One of the O 1s peaks (remarked O1) located at 530 eV for all samples is ascribed to the lattice oxygen of the O-Sn⁴⁺ bonds.¹⁷ While the higher binding energy peak in O 1s for the $\text{Sn}_{0.95}\text{Mn}_{0.05}\text{O}_2$ films reveals the presence of the chemisorbed O-containing species.^{9,20,21} The relatively high intensity of the “O_{chem}” component is due to the very high surface

sensitivity.²⁰ Based on the experimental and fitted XPS peak areas and their sensitivity factors, we quantitatively obtained a relative atomic concentration ratio O1:(Sn + Mn) of 1.93 for the $\text{Sn}_{0.95}\text{Mn}_{0.05}\text{O}_2$ with the $P_o = 10^{-4}$ Pa. Moreover, there is one marginal shoulder at about 527 eV from the O 1s signals for the $\text{Sn}_{0.95}\text{Fe}_{0.05}\text{O}_2$ films. It is probably formed by the iron oxides, as previously described by Yamashita and Hayes.²² On the other hand, the Mn $2p_{3/2}$ and Mn $2p_{1/2}$ peaks centered around 642.5 and 654 eV for the $\text{Sn}_{0.95}\text{Mn}_{0.05}\text{O}_2$ samples were the characteristics of Mn^{4+} .^{16,18} In the case of the Fe doped films, the Fe 2p region is divided into the Fe $2p_{1/2}$ peak at 726 eV and Fe $2p_{3/2}$ peak at 711.5 eV, corresponding to the Fe^{3+} feature. Furthermore, the Fe $2p_{3/2}$ peak has associated satellite peaks at 715.8 eV, which is clearly distinguishable from Fig. 3(c). The presence of the satellite peak may be due to the existence of Fe^{2+} .²² Then the Fe element seems to behave as mixed valences of Fe^{2+} and Fe^{3+} situated in the tetragonal $\text{Sn}_{0.95}\text{Fe}_{0.05}\text{O}_2$ films. However, Grosvenor *et al.* reported that a peak with a binding energy of about 715 eV has been found in the XPS spectra of Fe_2O_3 .²³ The exact assignment of the peak is still an unresolved issue for the Fe doped SnO_2 material. Interestingly, the core level peaks of Sn 3d and TM 2p in the $\text{Sn}_{0.95}\text{Mn}_{0.05}\text{O}_2$ and $\text{Sn}_{0.95}\text{Fe}_{0.05}\text{O}_2$ films show a slight shift with the varied oxygen pressure and the contrasted changes could be observed under the low oxygen pressure region, which is induced by the doping behaviors. It again indicates the difference in the atomic environment surrounding incorporated TM ions, as seen in the XRD patterns. Note that all binding energy positions of the elements for the $\text{Sn}_{0.95}\text{TM}_{0.05}\text{O}_2$ films are summarized in Table I.

C. IR reflectance from the $\text{Sn}_{0.95}\text{TM}_{0.05}\text{O}_2$ films

In order to further clarify the influence of P_o on structural properties, IR reflectance spectra for the $\text{Sn}_{0.95}\text{TM}_{0.05}\text{O}_2$ films were measured. Compared to the sapphire substrate, the spectrum of the $\text{Sn}_{0.95}\text{Mn}_{0.05}\text{O}_2$ film with $P_o = 10^{-1}$ Pa in Fig. 5(a) indicates that the three intense peaks at about 248, 289, and 601 cm^{-1} can be assigned to the E_u transverse optical (TO) phonon modes,¹⁰ which are correlated to the vertical displacements of Sn and O ions.^{24,25} The A_{2u} phonon mode appears in the small band region of 450–500 cm^{-1} . The lattice vibrations and optical functions of the $\text{Sn}_{0.95}\text{TM}_{0.05}\text{O}_2$

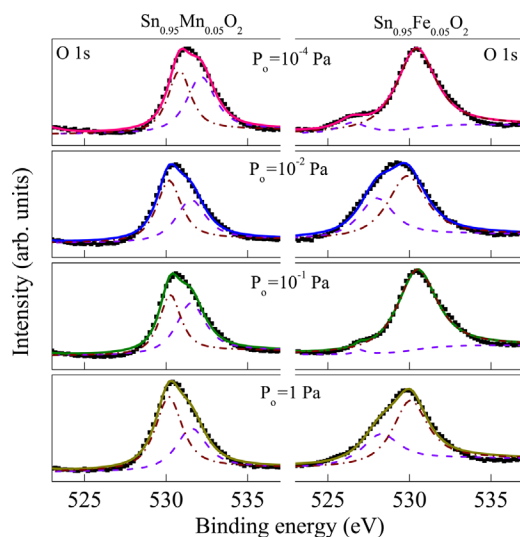


FIG. 4. (Color online) O 1s reference spectra of the $\text{Sn}_{0.95}\text{Mn}_{0.05}\text{O}_2$ (left) and $\text{Sn}_{0.95}\text{Fe}_{0.05}\text{O}_2$ (right) films as a function of oxygen pressure, respectively.

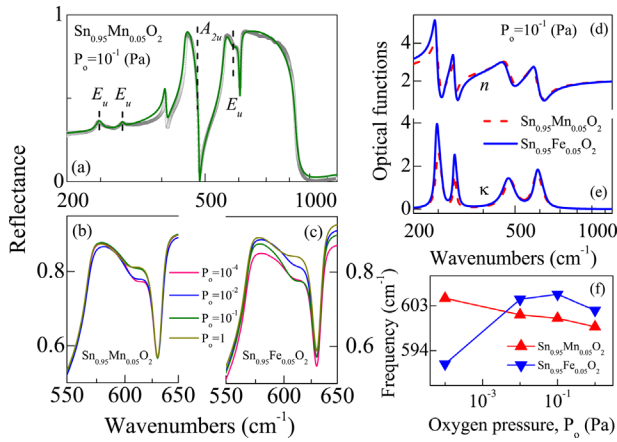


FIG. 5. (Color online) (a) Experimental infrared reflectance spectrum (dotted line) and the best-fit result (solid line) of the $\text{Sn}_{0.95}\text{Mn}_{0.05}\text{O}_2$ film grown under 10^{-1} Pa. The phonon modes can be clearly assigned by the dashed lines. (b) and (c) An enlarged frequency region of $550\text{--}650\text{ cm}^{-1}$ from the experimental reflectance spectra for the $\text{Sn}_{0.95}\text{TM}_{0.05}\text{O}_2$ (TM: Mn or Fe) films. (d) and (e) The doping effects on the optical functions of the $\text{Sn}_{0.95}\text{TM}_{0.05}\text{O}_2$ films deposited under the oxygen pressure of 10^{-1} Pa. The horizontal coordinate is the logarithmic unit to emphasize the lattice vibration region. (f) The corresponding variations with the oxygen pressure for the highest frequency E_u (TO) phonon modes.

films in the frequency range of $200\text{--}1200\text{ cm}^{-1}$ can be expressed using the Lorentz multi-oscillator model,

$$\tilde{\epsilon}(\omega) = \epsilon_{\infty, \text{IR}} + \sum_{k=1}^4 \frac{S_k \omega_{TO,k}^2}{\omega_{TO,k}^2 - \omega^2 - i\omega\Gamma_k}. \quad (1)$$

Here, $\epsilon_{\infty, \text{IR}}$, S_k , $\omega_{TO,k}$, Γ_k , and ω represent, in order, the high frequency dielectric constant, TO phonon strength, TO phonon frequency, the damping parameter of the TO phonon, and the frequency of the incident infrared light, respectively. A detailed theoretical consideration of the films can be found in Ref. 26. The former four fitting parameters ($\epsilon_{\infty, \text{IR}}$, S_k , $\omega_{TO,k}$, Γ_k) could be obtained from the fitting calculation and those values with the P_o are listed in Table II. As can be seen, the low E_u (TO) phonon frequencies are not strikingly changed corresponding to the P_o . However, the distinct deviations can be observed in the highest E_u (TO) vibration modes for the $\text{Sn}_{0.95}\text{TM}_{0.05}\text{O}_2$ systems, as exhibited in the panels (b), (c), and (f) of Fig. 5. With increasing the P_o , the highest frequency E_u (TO) phonon mode for the

$\text{Sn}_{0.95}\text{TM}_{0.05}\text{O}_2$ films shifts toward different frequency sides due to the doping elements and oxygen level, which can together contribute to the phonon characteristics. It should be emphasized that the optical functions of the $\text{Sn}_{0.95}\text{TM}_{0.05}\text{O}_2$ films can be uniquely determined by fitting the function model to the experimental data in the IR frequency region. For comparison, Fig. 5(d) and 5(e) display the variations of the refractive index n and extinction coefficient κ for the $\text{Sn}_{0.95}\text{TM}_{0.05}\text{O}_2$ samples deposited under the P_o of 10^{-1} Pa, respectively. The strengths of the low E_u (TO) frequencies in the $\text{Sn}_{0.95}\text{Fe}_{0.05}\text{O}_2$ film are stronger than those of the $\text{Sn}_{0.95}\text{Mn}_{0.05}\text{O}_2$ sample at the special pressure, suggesting that the Fe/Mn doping could differently affect the x-y plane movements and bond strength of Sn and O ions in SnO_2 system.²⁵ The behavior is a result of the doping effects on the crystalline and local lattice distortions, which was confirmed by the XRD measurements.

D. Transmittance properties of the $\text{Sn}_{0.95}\text{TM}_{0.05}\text{O}_2$ films

Optical characterization of the $\text{Sn}_{0.95}\text{TM}_{0.05}\text{O}_2$ films was performed over the UV-NIR photon energy range by measuring the transmittance of the films. Both $\text{Sn}_{0.95}\text{Mn}_{0.05}\text{O}_2$ and $\text{Sn}_{0.95}\text{Fe}_{0.05}\text{O}_2$ films exhibit the excellent transparency with spectral transmittance of about 80% in a NIR-visible wavelength region, as shown in the inset of Fig. 6. There are few interference oscillation periods in the transparent region due to the finite film thickness. Extrapolation from the linear parts of the transmission spectra in the strong absorption region yields the fundamental absorption edge, which was determined to be near 4 eV for the films. Besides a minor change in the transmittance lineshape due to the effects of P_o for the $\text{Sn}_{0.95}\text{Mn}_{0.05}\text{O}_2$ films, it can be also seen that the $\text{Sn}_{0.95}\text{Fe}_{0.05}\text{O}_2$ films have some sharp shoulders around the photon energy region of 2–4 eV since the 3d electrons form an impurity band in the forbidden band gap from the crystal field transition. It was reported that diffuse reflectance spectroscopy of Fe and Mn doped ZnO showed the existence of additional absorption bands, which were explained by the impurity d-band splitting model.²⁷ Furthermore, based on the first principle calculations, there are not only Fe-d states but also the oxygen 2p states staying at the Fermi level, induced by the Fe doping. It suggests the strong p-d coupling and hopping in Fe doped SnO_2 films. However, the phenomena

TABLE II. The Lorentz multi-oscillator parameter values for the $\text{Sn}_{0.95}\text{TM}_{0.05}\text{O}_2$ (TM: Mn or Fe) films with the varied oxygen pressure are extracted from the best fitting to infrared reflectance spectra in Fig. 5.

Samples	P_o (Pa)	$\epsilon_{\infty, \text{IR}}$	E_u			E_u			E_u			A_{2u}		
			S_1	$\omega_{TO,1}$ (cm^{-1})	Γ_1 (cm^{-1})	S_2	$\omega_{TO,2}$ (cm^{-1})	Γ_2 (cm^{-1})	S_3	$\omega_{TO,3}$ (cm^{-1})	Γ_3 (cm^{-1})	S_4	$\omega_{TO,4}$ (cm^{-1})	Γ_4 (cm^{-1})
A _{Mn}	10^{-4}	4.19	0.79	246	7.91	0.15	288	5.15	0.60	604	49.3	0.80	466	56.1
B _{Mn}	10^{-2}	4.29	0.78	247	8.66	0.15	288	5.56	0.72	601	53.5	0.70	468	53.3
C _{Mn}	10^{-1}	4.33	0.79	248	11.6	0.18	289	7.54	0.57	601	49.1	0.78	471	53.8
D _{Mn}	1	4.40	1.55	249	18.4	0.64	290	16.5	0.63	599	50.6	0.95	473	53.0
A _{Fe}	10^{-4}	4.11	0.55	246	6.99	0.11	288	4.36	1.14	591	73.1	0.87	457	47.2
B _{Fe}	10^{-2}	4.19	1.02	246	11.3	0.41	288	11.0	0.36	604	39.9	0.78	467	57.3
C _{Fe}	10^{-1}	4.32	1.14	245	8.67	0.38	288	8.39	0.57	605	43.8	0.85	464	55.7
D _{Fe}	1	4.59	1.36	248	13.7	0.40	288	11.3	0.29	602	27.3	0.98	473	51.7

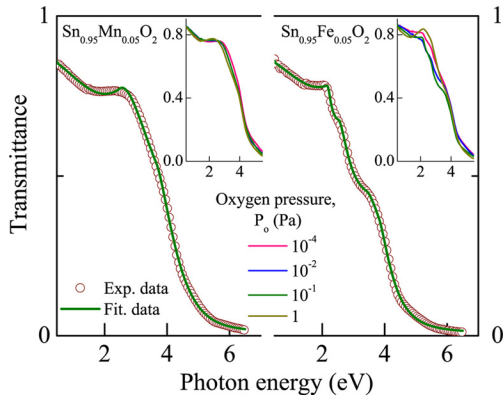


FIG. 6. (Color online) Experimental (dotted lines) and best-fit (solid lines) transmittance spectra taken from the $\text{Sn}_{0.95}\text{TM}_{0.05}\text{O}_2$ (TM: Mn or Fe) films with the oxygen pressure of 10^{-1} Pa. For clarity, the insets exhibit all experimental transmittance spectra of the films deposited under different oxygen pressure from ultraviolet to near-infrared photon energy region.

are weak in the case of Mn doping and consequently the shoulder transition related to the hybridization is also insignificant.⁵ On the other hand, oxygen vacancies play an important role in determining optical properties of the materials. When Fe substitutes Sn in the $\text{Sn}_{0.95}\text{Fe}_{0.05}\text{O}_2$ films, the octahedral environment may be varied if the oxygen vacancies are introduced in the first coordination sphere of Fe^{3+} .²⁸ It has been demonstrated that the Fe introduction largely facilitates the formation of oxygen vacancies.²⁹ Other data indicate that oxygen vacancy has a strong tendency to be close to the Fe ions, but the Mn ions have a small influence on the distribution of oxygen vacancy.⁵ So we attribute the appearance of those shoulders to the correlation between oxygen vacancies and dopant in the films, particularly the effects from the Fe contribution because of the distinct phenomenon in the $\text{Sn}_{0.95}\text{Fe}_{0.05}\text{O}_2$ films under the identical condition. It is evident that the different TM ions, together with the varied P_o , have a great influence on the oxygen vacancy distribution and then further result in different optical response behaviors.

Generally, the reliability of the fitting method mainly depends on the validity of the dielectric function model. It is a challenge to choose the most suitable model for material and the spectral range studied. There are some well-known dispersion functions, which are derived from the band parameters and can be used to express the optical response behavior.³⁰ Among them, the Tauc-Lorentz (TL) model is an available approach to describe the dielectric response of wide band gap materials in the NIR to UV range including the exciton effects. Moreover, the positions of electronic transitions can be accurately determined by the TL model, which are helpful to understand the absorption processes. The TL model can be derived from the Tauc joint density of states (DOS) and the standard quantum mechanical or Lorentz calculation for ϵ_2 (imaginary part of dielectric function) of a collection of non-interacting atoms.³¹ If the multiplied transitions are considered, ϵ_2 is written as

$$\epsilon_2(E) = \begin{cases} 0, & E \leq E_g \\ \frac{AE_0C(E - E_g)^2}{(E^2 - E_0^2)^2 + C^2E^2} \frac{1}{E}, & E > E_g \end{cases} \quad (2a)$$

The real part of the dielectric function ϵ_1 is given by Kramers-Krönig integration,

$$\epsilon_1(E) = \epsilon_{\infty,UV} + \frac{2}{\pi} P \int_{E_g}^{\infty} \frac{\xi \epsilon_2(\xi)}{\xi^2 - E^2} d\xi. \quad (2b)$$

Equation (2) depends on the following five parameters: the parameters A , E_0 , C correspond to the amplitude, the peak transition energy, and the broadening for the electronic transitions, respectively. The parameter E_g is the band gap energy and $\epsilon_{\infty,UV}$ is the high-frequency dielectric constant. The above TL dielectric function model has been successfully applied in many semiconductor and dielectric materials from the transparent to strong absorption region.^{32–35} It should be pointed out that the effect of the surface rough layer, whose value is much less than the film thickness, can be neglected in the evolution of the optical properties for the $\text{Sn}_{0.95}\text{TM}_{0.05}\text{O}_2$ films. Because relatively big light spot (about 4 mm in diameter) and vertical incident accessory are used in the present experiments, the transmittance spectra cannot be sensitive to the porous surface layer. Therefore, a three-phase layered structure (air/film/substrate) and the TL dielectric model were used to calculate the UV-NIR transmittance spectra of the $\text{Sn}_{0.95}\text{TM}_{0.05}\text{O}_2$ films.

The experimental transmittance curves and fitting data with the TL model for the $\text{Sn}_{0.95}\text{TM}_{0.05}\text{O}_2$ films grown under the P_o of 10^{-1} Pa are presented in the Fig. 6. Note that two TL dispersion functions are used for the $\text{Sn}_{0.95}\text{Mn}_{0.05}\text{O}_2$ and four TL dispersion functions are necessary for the $\text{Sn}_{0.95}\text{Fe}_{0.05}\text{O}_2$ films due to the distinguished shoulder structures. It reveals that more than one single type of electronic transitions dominate the optical absorption for the films,³⁵ and the Fe introduction can cause the shoulder patterns to become much stronger. The TL parameters obtained from the fitting are summarized in Table III. It can be seen that the $\epsilon_{\infty,UV}$ is smaller than the $\epsilon_{\infty,IR}$ because the physical parameter accounts for the so-called high-frequency limit. Nevertheless, the values of both $\epsilon_{\infty,UV}$ and $\epsilon_{\infty,IR}$ are well located in a reasonable magnitude region, as compared with some typical wide band gap semiconductors and insulators. Correspondingly, it indicates that the contributions from the high energy electronic transition for the films in the IR region are remarkable compared with that in the UV-NIR region. As an example, the optical functions for the $\text{Sn}_{0.95}\text{TM}_{0.05}\text{O}_2$ films deposited under the P_o of 10^{-1} Pa are plotted in the left panel of Fig. 7, showing a normal dispersion in both Fe and Mn doped films. It is found that, at any pressure of the present work, the n for the $\text{Sn}_{0.95}\text{Mn}_{0.05}\text{O}_2$ films is larger than that of the $\text{Sn}_{0.95}\text{Fe}_{0.05}\text{O}_2$ films in mostly all studied photon energy region of 0.47–6.5 eV (not shown). Moreover, at the limited energy of 0.47 eV, the n values approximately vary from 2.07 to 2.10 and from 1.88 to 2 corresponding to different P_o for the $\text{Sn}_{0.95}\text{Mn}_{0.05}\text{O}_2$ and $\text{Sn}_{0.95}\text{Fe}_{0.05}\text{O}_2$ films, respectively. The deviation implies that the optical functions of the $\text{Sn}_{0.95}\text{TM}_{0.05}\text{O}_2$ films are very sensitive to the experimental oxygen level and doping effects, which could induce the corresponding crystalline and band structure change. From the right panel of Fig. 7, the E_{01} transition in the $\text{Sn}_{0.95}\text{Mn}_{0.05}\text{O}_2$ films decreases with increasing P_o and approaches the

TABLE III. The Tauc-Lorentz's parameter values for the $\text{Sn}_{0.95}\text{TM}_{0.05}\text{O}_2$ (TM: Mn or Fe) films are determined from the simulation to ultraviolet-near-infrared transmittance spectra in Fig. 6.

Samples	P_o (Pa)	Thickness (nm)	$\epsilon_{\infty,UV}$	TL ₁				TL ₂				TL ₃				TL ₄			
				A_1 (eV)	E_{01} (eV)	C_1 (eV)	E_{g1} (eV)	A_2 (eV)	E_{02} (eV)	C_2 (eV)	E_{g2} (eV)	A_3 (eV)	E_{03} (eV)	C_3 (eV)	E_{g3} (eV)	A_4 (eV)	E_{04} (eV)	C_4 (eV)	E_{g4} (eV)
A _{Mn}	10^{-4}	75	2.75	50.6	2.249	3.18	2.57	148	3.968	4.06	3.37	—	—	—	—	—	—	—	
B _{Mn}	10^{-2}	76	2.59	56.0	2.219	3.14	2.52	145	4.054	3.74	3.69	—	—	—	—	—	—	—	
C _{Mn}	10^{-1}	78	2.54	51.9	2.200	3.11	2.50	117	4.514	4.34	3.63	—	—	—	—	—	—	—	
D _{Mn}	1	90	2.75	27.6	2.261	3.20	2.26	128	4.327	3.67	3.65	—	—	—	—	—	—	—	
A _{Fe}	10^{-4}	93	2.03	37.7	1.838	0.45	2.12	59.7	2.014	1.06	2.58	88.1	2.840	4.01	3.40	132	3.102	3.65	3.76
B _{Fe}	10^{-2}	75	1.88	34.6	1.950	0.65	2.09	63.2	2.246	0.96	2.56	126	2.778	3.93	3.42	111	3.892	3.97	3.73
C _{Fe}	10^{-1}	91	2.22	53.0	2.107	0.27	2.16	72.8	2.249	0.70	2.52	116	2.974	4.21	3.41	136	3.456	1.97	3.81
D _{Fe}	1	119	2.32	27.3	1.902	0.27	2.14	43.7	2.076	2.94	2.61	55.8	2.950	4.17	3.41	178	3.209	4.54	3.77

minimum at the P_o of 10^{-1} Pa, then increases with further increasing P_o . But a distinct trend occurs in both E_{01} and E_{02} for the $\text{Sn}_{0.95}\text{Fe}_{0.05}\text{O}_2$ films due to the different dopants. As previously discussed, the varied P_o results in the change of electronic band structures and strongly affects the interband transition properties of the films. Thus, the optical transmittance of the Fe and Mn doped systems depend on different TM dopants and varied P_o parameters.

E. Oxygen pressure effects on photoluminescence emissions

To further explore the influence of P_o on structures, defects, and impurities in nanostructures, PL experiments of the $\text{Sn}_{0.95}\text{TM}_{0.05}\text{O}_2$ films were done at room temperature. As illustrated in Fig. 8, there are some broadening emission bands between 1 and 3.5 eV with the maximum at about 2.2 eV, which is close to the reported ones^{9,26} and the experimental data for the undoped SnO_2 films (not shown). It can be seen that there are three obvious peaks in the spectra of the films, including the emissions from SnO_2 and TM contributions, respectively. In order to determine the peak positions of emissions, a three peak fit of the PL spectra was carried out by Gaussian curve and the positions with varied

P_o were listed in Table I. As a comparison between the pure SnO_2 and $\text{Sn}_{0.95}\text{TM}_{0.05}\text{O}_2$ systems, besides the main peaks ($P_{\text{TM}-1}$ and $P_{\text{TM}-2}$) characterized by a broadening feature around 2.2 eV with a small emission shoulder at 1.9 eV, there is a sharp peak ($P_{\text{Mn}-3}$) centered at near 1.5 eV owing to the Mn introduction in the $\text{Sn}_{0.95}\text{Mn}_{0.05}\text{O}_2$ films.²⁶ Moreover, for the pure SnO_2 and $\text{Sn}_{0.95}\text{Mn}_{0.05}\text{O}_2$ films, the behavior that intensity reduction with increasing the oxygen pressure of the main peaks could be due to the similar P_o effect on the PL mechanism. Although the Mn composition is kept as a constant, the position and intensity of the $P_{\text{Mn}-3}$ are quite sensitive to the P_o . It indicates that the variations are a result of different P_o values, which affects the d electronic configuration induced by the Mn doping. It is widely believed that PL emission band centered in the range of 580–630 nm (2.14–1.97 eV) for SnO_2 nanostructures are derived from oxygen vacancy centers or surface states (e.g., tin vacancies/interstitials).^{11,36} But the exact mechanism of these bands is still controversial.

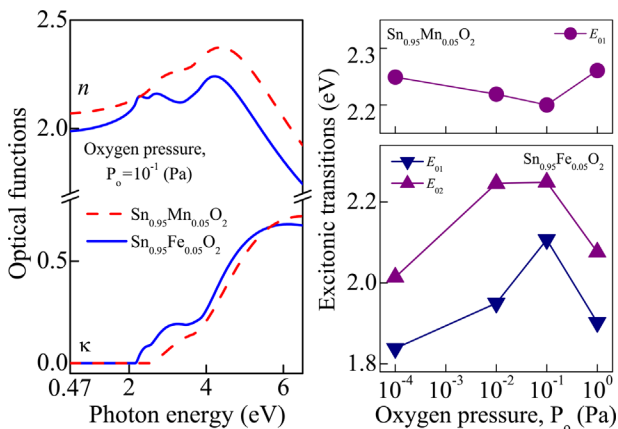


FIG. 7. (Color online) The left panel shows the refractive index n and the extinction coefficient κ for the $\text{Sn}_{0.95}\text{TM}_{0.05}\text{O}_2$ (TM: Mn or Fe) films grown under the oxygen pressure of 10^{-1} Pa. The right panel shows the variation trends of the electronic transition energies from the Tauc-Lorentz's parameters with the oxygen pressure.

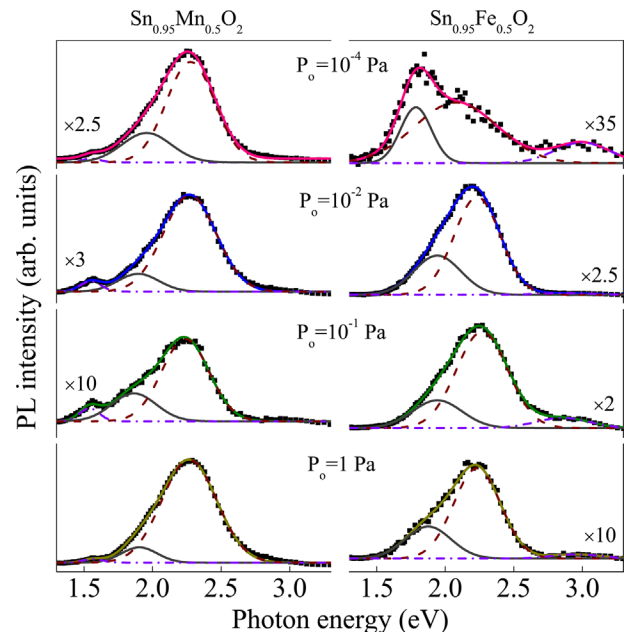


FIG. 8. (Color online) A three peak fitting of the photoluminescence spectra for the $\text{Sn}_{0.95}\text{TM}_{0.05}\text{O}_2$ (TM: Mn or Fe) films grown under different oxygen pressure. Note that some spectral lineshapes are enlarged by several times for a comparison.

In the present case, a possible explanation for the P_{TM-1} and P_{TM-2} of both pure SnO_2 and $\text{Sn}_{0.95}\text{TM}_{0.05}\text{O}_2$ films is that the electrons in the conduction band first relax nonradiatively to the defect states and then radiatively recombine with the holes in the valence band of SnO_2 , as argued in the $\text{SnO}_2/\text{p-Si}$ heterojunctions.³⁷ The conclusion has been confirmed by PL spectra using different excitations (325 and 488 nm) for SnO_2 nanowires.⁸ The mechanism of above emissions should be associated with the defects, which act as trapped states within the band gap of SnO_2 . There are various types of the defects, such as oxygen vacancies, tin vacancies, or tin interstitials, which give rise to different trapped states and contribute to the emission bands discussed above. Most commonly the oxygen vacancies exist with three different states (V_o^0 , V_o^+ , V_o^{++}). The V_o^0 center as very shallow donor, is very close to the conduction band edge and can capture electrons then form ionized vacancies.^{8,38,39} The presence of V_o^+ has been reported and confirmed by electron paramagnetic resonance study on SnO_2 .³⁸ It is expected that the P_{TM-1} or P_{TM-2} emission occurs due to the V_o^+ acceptor state. The P_{TM-2} may be due to the presence of isolated V_o^+ centers, which lies in a higher energy in the band gap than the complex V_o^+ centers producing the P_{TM-1} emission.⁸ Additionally, the P_{Fe-3} around 2.9 eV for the $\text{Sn}_{0.95}\text{Fe}_{0.05}\text{O}_2$ films can be assumed to the conduction band-acceptor or donor-acceptor transitions owing to the formation of V_o^{++} luminescent center.^{8,38} On the other hand, the oxygen vacancies interact with interfacial tin vacancies and lead to a considerable amount of trapped states within the band gap, then result in the PL emission signal.¹¹ Zhang *et al.* reported that the strong emission at 554 nm (2.2 eV) was likely related to the oxygen vacancy and the shoulder at 625 nm (1.98 eV) may be related to tin interstitials.⁹ One also suggested that the observed peak at 2.1 eV is from the unoccupied electron states in the dangling bonds at the surface of SnO_2 crystals.⁴⁰ These mentioned defect states are complex and can be influenced by the growth conditions.

The dependence of the corresponding intensity and emission peak positions on the parameter P_o is presented in Fig. 9 for the $\text{Sn}_{0.95}\text{Mn}_{0.05}\text{O}_2$ and $\text{Sn}_{0.95}\text{Fe}_{0.05}\text{O}_2$ films, respectively. The intensity at the P_{TM-2} emission decreases as increasing P_o , then the minimum is obtained for the P_o of 10^{-1} Pa in the $\text{Sn}_{0.95}\text{Mn}_{0.05}\text{O}_2$ films, showing a remarkable response to oxygen level. In contrast, there is an opposite trend below and above the P_o of 10^{-1} Pa for the $\text{Sn}_{0.95}\text{Fe}_{0.05}\text{O}_2$ films. As we know, the oxygen vacancies can be present for the oxide materials during the PLD process. Supposed that the lower P_o means less oxygen content, then a large amount of oxygen vacancies are supplied by the surrounding oxygen. Therefore, the intensity of the peak, which is related to oxygen vacancies acted as the defect states, decreases with increasing P_o . The similar situation can be seen in Fig. 9 for the $\text{Sn}_{0.95}\text{Mn}_{0.05}\text{O}_2$ films until the pressure reaches 10^{-1} Pa. Further evidence on the relation between oxygen vacancies and intensity of the peak emission for SnO_2 nanostructures deposited at different oxygen flow rate has been found.⁹ It could be concluded that the less oxygen vacancies in the crystal can result in a weaker peak intensity, which again confirms the above emission mechanism. However, a different sign of the intensity in the $\text{Sn}_{0.95}\text{Fe}_{0.05}\text{O}_2$

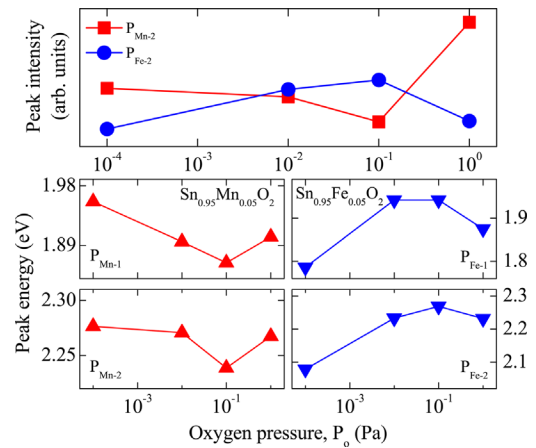


FIG. 9. (Color online) The oxygen pressure dependence of photoluminescence intensities and peak positions for the $\text{Sn}_{0.95}\text{TM}_{0.05}\text{O}_2$ (TM: Mn or Fe) films. It indicates that there are different variation trends for Mn or Fe doped SnO_2 materials with the oxygen pressure.

films may be explained by the fact that increasing oxygen vacancies, whose formation would be facilitated by the Fe presence,²⁹ cause the enhancement of relative intensity for P_{Fe-2} . Furthermore, the doping elements result in different structure evolution, which is indicated by XRD and IR reflectance measurements, and also could greatly affect the luminescence properties. From those views, the incorporation of Fe ion can be assumed as the dominant factor in the different PL phenomenon. So the effects, resulting from the Fe dopant and increased oxygen vacancies, together lead to the different optical activity for the $\text{Sn}_{0.95}\text{Fe}_{0.05}\text{O}_2$ films.

Note that the positions of P_{TM-1} and P_{TM-2} for the $\text{Sn}_{0.95}\text{TM}_{0.05}\text{O}_2$ films shift with increasing P_o and the corresponding trends coincide with those of PL intensities and E_{01} electronic transitions presented previously. Moreover, an interesting comparison can be made that these positions closely match the values of E_{01} and E_{02} transition energies determined from the TL model calculation, where the variations with the P_o values have the same inflection point. It indicates that the varied P_o not only modify the oxygen vacancy but also affect energy level of the TM ions, which are located in the band gap of SnO_2 . Therefore, one may suggest that the variation trends of electronic and optical properties with the P_o for the $\text{Sn}_{0.95}\text{Mn}_{0.05}\text{O}_2$ and $\text{Sn}_{0.95}\text{Fe}_{0.05}\text{O}_2$ systems could be different. It was reported that the absorption edge of SnO_2 has been assigned to interband transitions from the valence band edge with O 2p orbitals to the conduction band edge with Sn 5s orbitals.^{41,42} In TM (Fe or Mn) doped rutile SnO_2 , O ions around TM ions form an octahedral crystal field, splitting 3d orbitals into lower t_{2g} states and upper e_g states. From previously discussed, strong p-d hybridization in the $\text{Sn}_{0.95}\text{Fe}_{0.05}\text{O}_2$ films has been found, showing not only d states but also the oxygen 2p states staying at the Fermi level. However, they are weak in the Mn doped case.⁵ In addition, the interband electronic transitions are related to the ability of electrons located in bands below the Fermi level to be excited to unoccupied levels above it, and their intensity is proportional to the density of states.⁴³ Based on the first principle calculations, the DOS at the Fermi level is mainly derived from the O 2p states and only less than half

of the total states were contributed by Fe 3d states for $\text{Fe}_{0.125}\text{Sn}_{0.875}\text{O}_2$. It indicates that the strong p-d hybridization exist when the 3d electrons form an impurity induced by Fe, which is essential to mediate the exchange interaction between the doped TM ions.⁴⁴ Furthermore, Fe-O-Fe groups are common in the $\text{Sn}_{0.95}\text{Fe}_{0.05}\text{O}_2$ system, but are not easily formed in the $\text{Sn}_{0.95}\text{Mn}_{0.05}\text{O}_2$ film. Such special Fe-O-Fe bond and its distortion are expected to originate from the strong p-d hybridization and the smaller substitutional Fe ion radius (0.65 Å) compared with the Sn^{4+} (0.72 Å).^{10,44,45} In addition, it should be also noted that the ionic radius of Mn^{4+} (0.53 Å) is even smaller than that of Sn^{4+} .¹⁶ Thus, the different doping elements could intensely affect the electronic band structure of the SnO_2 matrix. Also, the P_o variation can affect oxygen content in the oxide films, then affect the O 2p and Fe/Mn 3d orbital distributions, which will induce the t_{2g} and e_g states located at different level in the energy space. It further results in different spectral response behavior with the doping in the varied P_o region due to the mutual interaction between TM ion and O levels. Hence, it could be understood that the electronic band and optical properties for the $\text{Sn}_{0.95}\text{TM}_{0.05}\text{O}_2$ films strongly correlate with the energy levels of dopants in the SnO_2 lattice, the d electronic configuration, and the distribution of oxygen vacancy derived from the P_o .

IV. CONCLUSION

To summarize, the oxygen pressure effects on the electronic band structures and optical properties of the $\text{Sn}_{0.95}\text{TM}_{0.05}\text{O}_2$ (TM: Mn or Fe) films have been determined by comprehensive characterizations. XRD analysis shows that the films are of the rutile structure and the variant P_o dependence of the structure parameters is due to the Mn or Fe elements contributions. The core level peaks of the $\text{Sn}_{0.95}\text{TM}_{0.05}\text{O}_2$ films from the XPS spectra indicate the difference in the atomic environment surrounding incorporated TM ions. The shoulder features in transmittance spectra can be observed, especially for the $\text{Sn}_{0.95}\text{Fe}_{0.05}\text{O}_2$ film, which can be attributed to the stronger p-d hybridization induced by the Fe doping. There are the distinct trends in the transition energies with the P_o for the $\text{Sn}_{0.95}\text{Mn}_{0.05}\text{O}_2$ and $\text{Sn}_{0.95}\text{Fe}_{0.05}\text{O}_2$ films owing to different correlation between TM ion and O level. Moreover, from the PL spectra, two main peaks for the films are ascribed to the defect states acted as trapping centers in the band gap. The PL intensities and positions have the corresponding change patterns with the diverse P_o values. This is because varied oxygen contents, different dopants, and the strong mutual interaction could induce the adjustment in the electronic band structure of the host oxide and contribute to PL emissions. The present results show the important roles of oxygen pressure and dopants in modifying optical properties and luminescence experiments for the $\text{Sn}_{0.95}\text{TM}_{0.05}\text{O}_2$ films at low temperatures are necessary in next work to further clarify the physical behavior.

ACKNOWLEDGMENTS

This work was financially supported by Natural Science Foundation of China (Grant Nos. 60906046 and 11074076),

Major State Basic Research Development Program of China (Grant Nos. 2007CB924901 and 2011CB922200), Program of New Century Excellent Talents, MOE (Grant No. NCET-08-0192), and PCSIRT, Projects of Science and Technology Commission of Shanghai Municipality (Grant Nos. 10DJ1400201, 10SG28, 11520701300, 10ZR1409800, and 09ZZ42), The Program for Professor of Special Appointment (Eastern Scholar) at Shanghai Institutions of Higher Learning. One of the authors (W.L.Y.) thanks the Project of East China Normal University (Grant No. CX2011005).

- ¹J. H. He, T. H. Wu, C. L. Hsin, K. M. Li, L. J. Chen, Y. L. Chueh, L. J. Chou, and Z. L. Wang, *Small* **2**, 116 (2007).
- ²J. Q. Hu, Y. S. Bando, Q. L. Liu, and D. Golberg, *Adv. Funct. Mater.* **13**, 493 (2003).
- ³C. V. Komen, A. Thurber, K. M. Reddy, J. Hay, and A. Punnoose, *J. Appl. Phys.* **103**, 07D141 (2008).
- ⁴C. B. Fitzgerald, M. Venkatesan, L. S. Dorneles, R. Gunning, P. Stamenov, J. M. D. Coey, P. A. Stampe, R. J. Kennedy, E. C. Moreira, and U. S. Sias, *Phys. Rev. B* **74**, 115307 (2006).
- ⁵X. L. Wang, Z. X. Dai, and Z. Zeng, *J. Phys.: Condens. Matter* **20**, 045214 (2008).
- ⁶M. Gaidi, A. Hajjaji, R. Smirani, B. Bessais, and M. A. El Khakani, *J. Appl. Phys.* **108**, 063537 (2010).
- ⁷F. Trani, M. Causà, D. Ninno, G. Cantele, and V. Barone, *Phys. Rev. B* **77**, 245410 (2008).
- ⁸A. Kar, M. A. Stroschio, M. Dutta, J. Kumari, and M. Meyyappan, *Semicond. Sci. Technol.* **25**, 024012 (2010).
- ⁹L. Zhang, S. H. Ge, Y. L. Zuo, B. M. Zhang, and L. Xi, *J. Phys. Chem. C* **114**, 7541 (2010).
- ¹⁰W. L. Yu, K. Jiang, J. D. Wu, J. Gan, M. Zhu, Z. G. Hu, and J. H. Chu, *Phys. Chem. Chem. Phys.* **13**, 6211 (2011).
- ¹¹W. C. Zhou, R. B. Liu, Q. Wan, Q. L. Zhang, A. L. Pan, L. Guo, and B. S. Zou, *J. Phys. Chem. C* **113**, 1719 (2009).
- ¹²B. J. Jin, S. H. Bae, S. Y. Lee, and S. Im, *Mater. Sci. Eng. B* **71**, 301 (2000).
- ¹³A. Thurber, K. M. Reddy, and A. Punnoose, *J. Appl. Phys.* **105**, 07E706 (2009).
- ¹⁴S. J. Rani, S. C. Roy, N. Karar, and M. C. Bhatnagar, *Solid State Commun.* **141**, 214 (2007).
- ¹⁵C. B. Fitzgerald, M. Venkatesan, A. P. Douvalis, S. Huber, J. M. D. Coey, and T. Bakas, *J. Appl. Phys.* **95**, 7390 (2004).
- ¹⁶L. B. Duan, G. H. Rao, J. Yu, Y. C. Wang, G. Y. Liu, and J. K. Liang, *J. Appl. Phys.* **101**, 063917 (2007).
- ¹⁷L. Yan, J. S. Pan, and C. K. Ong, *Mater. Sci. Eng. B* **128**, 34 (2006).
- ¹⁸L. S. Wei, J. H. Li, and X. F. Tang, *Catal. Lett.* **127**, 107 (2009).
- ¹⁹C. Körber, J. Suffner, and A. Klein, *J. Phys. D: Appl. Phys.* **43**, 055301 (2010).
- ²⁰A. Kolmakov, S. Potluri, A. Barinov, T. O. Montes, L. Gregoratti, M. A. Niño, A. Locatelli, and M. Kiskinova, *ACS Nano* **2**, 1993 (2008).
- ²¹S. Bazargan, N. F. Heinig, D. Pradhan, and K. T. Leung, *Cryst. Growth Des.* **11**, 247 (2011).
- ²²T. Yamashita and P. Hayes, *Appl. Surf. Sci.* **254**, 2441 (2008).
- ²³A. P. Grosvenor, B. A. Kobe, M. C. Biesinger, and N. S. McIntyre, *Surf. Interface Anal.* **36**, 1564 (2004).
- ²⁴T. Hirata, K. Ishioka, M. Kitajima, and H. Doi, *Phys. Rev. B* **53**, 8442 (1996).
- ²⁵H. Zhang, Y. L. Liu, K. Zhu, G. G. Siu, Y. H. Xiong, and C. S. Xiong, *J. Phys.: Condens. Matter* **10**, 11121 (1998).
- ²⁶W. L. Yu, W. W. Li, J. D. Wu, J. Sun, J. J. Zhu, M. Zhu, Z. G. Hu, and J. H. Chu, *J. Phys. Chem. C* **114**, 8593 (2010).
- ²⁷S. Singh and M. S. Ramachandra Rao, *Phys. Rev. B* **80**, 045210 (2009).
- ²⁸A. I. Rykov, K. Nomura, J. Sakuma, C. Barrero, Y. Yoda, and T. Mitsui, *Phys. Rev. B* **77**, 014302 (2008).
- ²⁹A. Roldán, M. Boronat, A. Corma, and F. Illas, *J. Phys. Chem. C* **114**, 6511 (2010).
- ³⁰A. B. Djurišić, Y. Chan, and E. H. Li, *Mater. Sci. Eng. R* **38**, 237 (2002).
- ³¹G. E. Jellison and F. A. Modine, *Appl. Phys. Lett.* **69**, 371 (1996); **69**, 2137 (1996).
- ³²W. W. Li, J. J. Zhu, J. D. Wu, J. Gan, M. Zhu, Z. G. Hu, and J. H. Chu, *Appl. Phys. Lett.* **97**, 121102 (2010).

- ³³C. Ke, Z. Yang, W. Zhu, J. S. Pan, and S. Karamat, *J. Appl. Phys.* **107**, 013515 (2010).
- ³⁴P. Chen, N. J. Podraza, X. S. Xu, A. Melville, E. Vlahos, V. Gopalan, R. Ramesh, D. G. Schlom, and J. L. Musfeldt, *Appl. Phys. Lett.* **96**, 131907 (2010).
- ³⁵L. Y. Liang, Z. M. Liu, H. T. Cao, Y. Y. Shi, X. L. Sun, Z. Yu, A. H. Chen, H. Z. Zhang, and Y. Q. Fang, *ACS Appl. Mater. Interfaces* **2**, 1565 (2010).
- ³⁶H. T. Chen, X. L. Wu, S. J. Xiong, W. C. Zhang, and J. Zhu, *Appl. Phys. A* **97**, 365 (2009).
- ³⁷Z. Z. Yuan, D. S. Li, M. H. Wang, P. L. Chen, D. R. Gong, P. H. Cheng, and D. R. Yang, *Appl. Phys. Lett.* **92**, 121908 (2008).
- ³⁸S. Das, S. Kar, and S. Chaudhuri, *J. Appl. Phys.* **99**, 114303 (2006).
- ³⁹K. Nagaveni, M. S. Hegde, and G. Madras, *J. Phys. Chem. B* **108**, 20204 (2004).
- ⁴⁰J. X. Zhou, M. S. Zhang, J. M. Hong, and Z. Yin, *Solid State Commun.* **138**, 242 (2006).
- ⁴¹K. C. Mishra, K. H. Johnson, and P. C. Schmidt, *Phys. Rev. B* **51**, 13972 (1995).
- ⁴²Ph. Barbarat, S. F. Matar, and G. Le. Blevennec, *J. Mater. Chem.* **7**, 2547 (1997).
- ⁴³F. Yubero, V. M. Jiménez, and A. R. González-Elipe, *Surf. Sci.* **400**, 116 (1998).
- ⁴⁴S. J. Hu, S. S. Yan, X. X. Yao, Y. X. Chen, G. L. Liu, and L. M. Mei, *Phys. Rev. B* **75**, 094412 (2007).
- ⁴⁵X. Mathew, J. P. Enriquez, C. Mejía-García, G. Contreras-Puente, M. A. Cortes-Jacome, J. A. Toledo Antonio, J. Hays, and A. Punnoose, *J. Appl. Phys.* **100**, 073907 (2006).